

Class-Distinct and Class-Mutual Image Generation with GANs

Takuhiro Kaneko¹
t.kaneko@mi.t.u-tokyo.ac.jp

Yoshitaka Ushiku¹
ushiku@mi.t.u-tokyo.ac.jp

Tatsuya Harada^{1,2}
harada@mi.t.u-tokyo.ac.jp

¹ Graduation School of
Information Science and Technology
The University of Tokyo
Tokyo, Japan

² RIKEN Center for
Advanced Intelligence Project
Tokyo, Japan

Abstract

Class-conditional extensions of generative adversarial networks (GANs), such as auxiliary classifier GAN (AC-GAN) and conditional GAN (cGAN), have garnered attention owing to their ability to decompose representations into class labels and other factors and to boost the training stability. However, a limitation is that they assume that each class is separable and ignore the relationship between classes even though class overlapping frequently occurs in a real-world scenario when data are collected on the basis of diverse or ambiguous criteria. To overcome this limitation, we address a novel problem called class-distinct and class-mutual image generation, in which the goal is to construct a generator that can capture between-class relationships and generate an image selectively conditioned on the class specificity. To solve this problem without additional supervision, we propose classifier’s posterior GAN (CP-GAN), in which we redesign the generator input and the objective function of AC-GAN for class-overlapping data. Precisely, we incorporate the classifier’s posterior into the generator input and optimize the generator so that the classifier’s posterior of generated data corresponds with that of real data. We demonstrate the effectiveness of CP-GAN using both controlled and real-world class-overlapping data with a model configuration analysis and comparative study. Our code is available at <https://github.com/takuhirok/CP-GAN/>.

1 Introduction

In computer vision and machine learning, generative adversarial networks (GANs) [1] have become a prominent model owing to their ability to represent high-dimensional data in a compact latent space and to generate high-fidelity data [2, 20, 21, 56, 59]. In particular, class-conditional extensions of GANs (*e.g.*, auxiliary classifier GAN (AC-GAN) [33] and conditional GAN (cGAN) [34, 35]) have garnered attention owing to their two strong properties: (1) The supervision of class labels makes it possible to decompose representations into class labels and other factors. This allows the generator to generate an image selectively conditioned on class labels [17, 18, 34, 35, 38, 60]. (2) The additional information simplifies the learned target from an overall distribution to the class-conditional distributions. This contributes to stabilize the GAN training [4, 35, 38, 59].

However, a limitation is that they assume that each class is separable and ignore the relationship between classes. This not only restricts applications but also causes difficulty

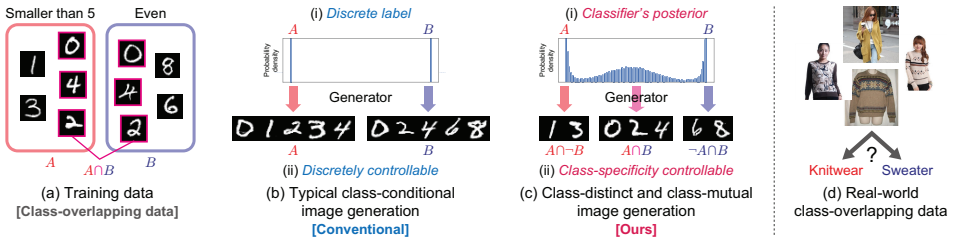


Figure 1: Example of class-distinct and class-mutual image generation. Given class-overlapping data (a), a typical class-conditional image generation model (e.g., AC-GAN; (b)) is optimized conditioned on discrete labels (b-i) and generates data of each class separately (b-ii). In contrast, our class-distinct and class-mutual image generation model (i.e., CP-GAN; (c)) represents between-class relationships in the generator input using the classifier’s posterior (c-i) and generates an image conditioned on the class specificity (c-ii). Classes frequently overlap in a real-world scenario when classes are confusing (d).

in modeling class-overlapping data even though class overlapping frequently occurs in a real-world scenario when data are collected on the basis of diverse or ambiguous criteria. Figure 1 shows an example. In Figure 1(a), class A includes digits that are smaller than five and class B contains even digits. In this case, “0,” “2,” and “4” belong to both classes. Given such *class-overlapping* data, a typical class-conditional image generation model (e.g., AC-GAN [8]) is optimized conditioned on *discrete* labels (Figure 1(b-i)) and generates data of each class *separately* (Figure 1(b-ii)) without considering the between-class relationships.

To remedy this drawback, we address a novel problem called *class-distinct and class-mutual image generation*, in which the goal is to construct a generator that can capture between-class relationships and generate an image selectively on the basis of the *class specificity*. To solve this problem without additional supervision, we propose *classifier’s posterior GAN (CP-GAN)*, in which we redesign the generator input and the objective function of AC-GAN for *class-overlapping* data. Precisely, we employ the classifier’s posterior to represent the between-class relationships and incorporate it into the generator input, as shown in Figure 1(c-i). Additionally, we optimize the generator so that the classifier’s posterior of generated data corresponds with that of real data. This formulation allows CP-GAN to capture the between-class relationships in a data-driven manner and to generate an image conditioned on the *class specificity*, as shown in Figure 1(c-ii).

To the best of our knowledge, class-distinct and class-mutual image generation is a novel task not sufficiently examined in previous studies. To advance this research, in the experiments, we introduce controlled class-overlapping data on CIFAR-10 [25] and report the benchmark performance with a model configuration analysis and comparative study. Classes frequently overlap in a real-world scenario when classes are confusing, as shown in Figure 1(d). Hence, we also evaluated CP-GAN using such real-world class-overlapping data.

Overall, our contributions are summarized as follows:

- We tackle a novel problem called *class-distinct and class-mutual image generation*: given *class-overlapping* data, the goal is to construct a generator that can capture between-class relationships and generate an image selectively conditioned on the *class specificity*.
- To solve this problem, we propose *CP-GAN*, in which we redesign the generator input and the objective function of AC-GAN for *class-overlapping* data. This formulation allows CP-GAN to solve this problem without additional supervision.
- We demonstrate the effectiveness of CP-GAN using both controlled and real-world class-overlapping data with a model configuration analysis and comparative study.

- As further analysis, we also demonstrate the generality of CP-GAN by applying it to image-to-image translation. See Appendix A for details.
- Our code is available at <https://github.com/takuhirok/CP-GAN/>.

2 Related work

Deep generative models. Along with GANs, prominent three deep generative models are variational autoencoders (VAEs) [23, 43], autoregressive models (ARs) [49], and flow-based models (Flows) [9]. All these models have pros and cons. A well-known weakness of GANs is training instability; however, this has been improved in recent work [11, 12, 13, 8, 14, 21, 22, 31, 33, 36, 39, 45, 51, 59, 62]. In this study, we focus on GANs owing to their flexibility in designing the latent space. This makes it easy to incorporate conditional information, such as our classifier’s posterior. Conditional extensions have been proposed for other models [24, 30, 42, 50, 55], and incorporating our ideas into them is a promising direction of future work.

Disentangled representation learning. Naive GANs do not have an explicit structure in the latent space. Hence, their latent variables may be used by the generator in a highly entangled manner. To solve this problem, recent studies have incorporated supervision into the networks [17, 18, 19, 34, 35, 38, 40, 41, 47, 52, 57, 58]. However, their learnable representations are restricted to the given supervision. To overcome this limitation, unsupervised [8, 18] and weakly supervised [17, 18, 29, 32] models have been also proposed. Our proposed CP-GAN is a weakly supervised model because it learns a *class-specificity* controllable model only using weak supervision (*i.e.*, *discrete* labels). The difference from the previous models is that CP-GAN incorporates *class specificity*. In this aspect, class-distinct and class-mutual image generation is different from typical *class-wise interpolation* (or category morphing in [55]) because the latter interpolates between classes regardless of class specificity. We empirically demonstrate this difference in Figure 9 in the Appendix. Additionally, We further discuss the relationships between CP-GAN and previous class-conditional extensions of GANs in Section 3.5.

3 Class-distinct and class-mutual image generation

3.1 Notations and problem statement

We first define notations and the problem statement. We use superscripts r and g to denote the real distribution and the generative distribution, respectively. Let $\mathbf{x} \in \mathcal{X}$ and $\mathbf{y} \in \mathcal{Y}$ be the image and the corresponding class label, respectively. Here, \mathcal{X} is the image space $\mathcal{X} \subseteq \mathbb{R}^d$, where d is the dimension of the image. \mathcal{Y} is the label space $\mathcal{Y} = \{\mathbf{y} : \mathbf{y} \in \{0, 1\}^c, \mathbf{1}^\top \mathbf{y} = 1\}$, where c is the number of classes and we use a one-hot vector form to represent labels. We address the *instance-dependent class overlapping*: class overlapping that occurs depending on the image content. In such a situation, *class-distinct* and *class-mutual* states are determined relying on the underlying class posterior $p^r(\mathbf{y}|\mathbf{x})$. For example, when $p^r(\mathbf{y}|\mathbf{x})$ is close to 1 for a specific class, \mathbf{x} is a *class-distinct* image. In contrast, when $p^r(\mathbf{y}|\mathbf{x})$ has some values for multiple classes, \mathbf{x} is a *class-mutual* image.

Our goal is, given *discretely* labeled data $(\mathbf{x}^r, \mathbf{y}^r) \sim p^r(\mathbf{x}, \mathbf{y})$, to construct a class-distinct and class-mutual image generator that can selectively generate an image conditioned on the *class specificity* (*i.e.*, $p^r(\mathbf{y}|\mathbf{x})$). This is challenging for typical conditional GANs because they learn a generator conditioned on the observable *discrete* \mathbf{y}^r and cannot incorporate the

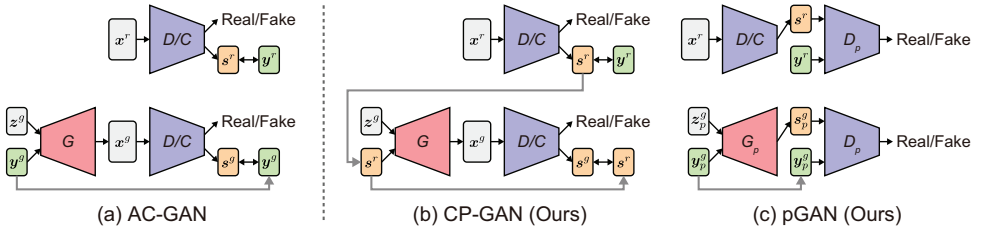


Figure 2: Comparison of AC-GAN (a) and CP-GAN (b). A green rectangle indicates a discrete label (or hard label), while an orange rectangle indicates a classifier’s posterior (or soft label). In CP-GAN, we redesign the generator input and the objective function of AC-GAN to construct a generator that is conditioned on the class specificity. CP-GAN requires a classifier’s posterior for real data (\mathbf{s}^r) for generating an image. To mitigate this requirement, we introduce pGAN (c) that learns a classifier’s posterior distribution.

class specificity. To solve this problem without additional supervision, we develop CP-GAN, in which we redesign the generator input and the objective function of AC-GAN, as shown in Figure 2(b). In the next sections, we review AC-GAN (which is the baseline of CP-GAN), clarify the limitations of AC-GAN in class-overlapping data, and introduce CP-GAN. Finally, we summarize the relationships with previous class-conditional extensions of GANs.

3.2 Baseline: AC-GAN

AC-GAN [58] is a class-conditional extension of GAN. Its aim is to learn a conditional generator G that transforms the noise \mathbf{z}^g and the label \mathbf{y}^g into the image \mathbf{x}^g , *i.e.*, $\mathbf{x}^g = G(\mathbf{z}^g, \mathbf{y}^g)$, where \mathbf{z}^g is the noise sampled from a normal distribution $p^g(\mathbf{z}) = \mathcal{N}(0, I)$ and \mathbf{y}^g is the class label sampled from a categorical distribution $p^g(\mathbf{y}) = \text{Cat}(K = c, p = 1/c)$. To achieve this aim, AC-GAN uses two losses, namely an adversarial loss [14] and auxiliary classifier (AC) loss [58]. We illustrate the AC-GAN architecture in Figure 2(a).

Adversarial loss. The adversarial loss is defined as

$$\mathcal{L}_{\text{GAN}} = \mathbb{E}_{\mathbf{x}^r \sim p^r(\mathbf{x})} [\log D(\mathbf{x}^r)] + \mathbb{E}_{\mathbf{z}^g \sim p^g(\mathbf{z}), \mathbf{y}^g \sim p^g(\mathbf{y})} [\log(1 - D(G(\mathbf{z}^g, \mathbf{y}^g)))] \quad (1)$$

where D is a discriminator that attempts to find the best decision boundary between the real images \mathbf{x}^r and the generated image $\mathbf{x}^g = G(\mathbf{z}^g, \mathbf{y}^g)$ by maximizing this loss, while G attempts to generate an image \mathbf{x}^g indistinguishable by D by minimizing this loss.

AC loss. The AC losses of real images and generated images are respectively defined as

$$\mathcal{L}_{\text{AC}}^r = \mathbb{E}_{(\mathbf{x}^r, \mathbf{y}^r) \sim p^r(\mathbf{x}, \mathbf{y})} [-\log C(\mathbf{y} = \mathbf{y}^r | \mathbf{x}^r)] = \mathbb{E}_{(\mathbf{x}^r, \mathbf{y}^r) \sim p^r(\mathbf{x}, \mathbf{y})} [-\mathbf{y}^{r\top} \log \mathbf{s}^r], \quad (2)$$

$$\mathcal{L}_{\text{AC}}^g = \mathbb{E}_{\mathbf{z}^g \sim p^g(\mathbf{z}), \mathbf{y}^g \sim p^g(\mathbf{y})} [-\log C(\mathbf{y} = \mathbf{y}^g | G(\mathbf{z}^g, \mathbf{y}^g))] = \mathbb{E}_{\mathbf{z}^g \sim p^g(\mathbf{z}), \mathbf{y}^g \sim p^g(\mathbf{y})} [-\mathbf{y}^{g\top} \log \mathbf{s}^g], \quad (3)$$

where $\mathbf{s}^r = C(\mathbf{y} | \mathbf{x}^r)$ and $\mathbf{s}^g = C(\mathbf{y} | G(\mathbf{z}^g, \mathbf{y}^g))$ are classifier’s posteriors (or soft labels) for a real image and generated image, respectively. By minimizing $\mathcal{L}_{\text{AC}}^r$, C learns to classify the real image \mathbf{x}^r to the corresponding class \mathbf{y}^r . Subsequently, G attempts to generate an image \mathbf{x}^g classified to the corresponding class \mathbf{y}^g , by minimizing $\mathcal{L}_{\text{AC}}^g$.

Full objective. In practice, shared networks between D and C are commonly used [14, 58]. In this configuration, the full objective is written as

$$\mathcal{L}_{D/C} = -\mathcal{L}_{\text{GAN}} + \lambda^r \mathcal{L}_{\text{AC}}^r, \quad \mathcal{L}_G = \mathcal{L}_{\text{GAN}} + \lambda^g \mathcal{L}_{\text{AC}}^g, \quad (4)$$

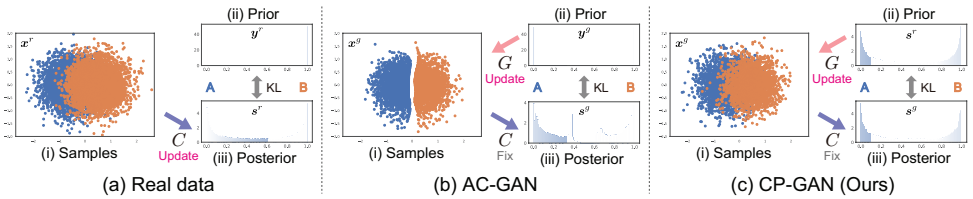


Figure 3: Comparison of training procedures in the AC losses. (a) In the AC loss of real data, C is optimized to capture the class overlapping state in \mathbf{x}^r (a-i). (b) In AC-GAN, G is optimized so that the classifier’s posterior for the generated data (\mathbf{s}^g ; b-iii) is close to the discrete prior (\mathbf{y}^g ; b-ii). This enforces G to generate class-separate data (b-i). (c) In contrast, in CP-GAN, G is optimized so that the classifier’s posterior for the generated data (\mathbf{s}^g ; c-iii) is close to the classifier’s posterior for the real data (\mathbf{s}^r ; c-ii). This allows G to generate class-overlapping data (c-i) that are close to real data (a-i).

where λ^r and λ^g are trade-off parameters between the adversarial loss and the AC loss for the real image and generated image, respectively. D/C and G are optimized by minimizing $\mathcal{L}_{D/C}$ and \mathcal{L}_G , respectively.

3.3 Limitations of AC-GAN in class-overlapping data

To explain the limitations of AC-GAN in class-overlapping data, we use a toy example: data that consist of two-class Gaussian distributions with class overlapping, as shown in Figure 3(a-i). Our goal is to construct a generative model that mimics these distributions. For an easy explanation, we rewrite the AC losses in Equations 2 and 3 as

$$\mathcal{L}_{\text{KL-AC}}^r = \mathbb{E}_{(\mathbf{x}^r, \mathbf{y}^r) \sim p^r(\mathbf{x}, \mathbf{y})} \mathcal{D}_{\text{KL}}(\mathbf{y}^r \| \mathbf{s}^r), \quad (5)$$

$$\mathcal{L}_{\text{KL-AC}}^g = \mathbb{E}_{\mathbf{z}^g \sim p^g(\mathbf{z}), \mathbf{y}^g \sim p^g(\mathbf{y})} \mathcal{D}_{\text{KL}}(\mathbf{y}^g \| \mathbf{s}^g), \quad (6)$$

where we rename the AC losses $\mathcal{L}_{\text{AC}}^r$ and $\mathcal{L}_{\text{AC}}^g$ as the KL-AC losses $\mathcal{L}_{\text{KL-AC}}^r$ and $\mathcal{L}_{\text{KL-AC}}^g$, respectively. Here, $\mathcal{D}_{\text{KL}}(\mathbf{y} \| \mathbf{s}) = \mathbf{y}^\top \log \mathbf{y} - \mathbf{y}^\top \log \mathbf{s}$ is the Kullback-Leibler (KL) divergence between \mathbf{y} and \mathbf{s} , where we represent the distributions in a vector form (*i.e.*, \mathbf{y} and \mathbf{s}). In practice, we ignore $\mathbf{y}^\top \log \mathbf{y}$ because it is constant when it is fixed (*e.g.*, given as the ground truth).

Both the KL-AC losses bring \mathbf{s}^r and \mathbf{s}^g close to \mathbf{y}^r and \mathbf{y}^g , respectively, in terms of the KL divergence; however, there is a difference for the optimization target. In $\mathcal{L}_{\text{KL-AC}}^r$, the input of C (*i.e.*, \mathbf{x}^r) is fixed and the parameters of C are optimized. Namely, the class overlapping state in \mathbf{x}^r is maintained during the training, as shown in Figure 3(a-i). This encourages the classifier’s posterior (\mathbf{s}^r) to be optimized to represent the class overlapping state (Figure 3(a-iii)) even when the ground truth class prior (\mathbf{y}^r) is discrete (Figure 3(a-ii)). In contrast, in $\mathcal{L}_{\text{KL-AC}}^g$, C is fixed and the input of C (*i.e.*, $\mathbf{x}^g = G(\mathbf{z}^g, \mathbf{y}^g)$) is optimized. Unlike in $\mathcal{L}_{\text{KL-AC}}^r$, there is no restriction that promotes G to follow the class overlapping state. As a result, the classifier’s posterior (\mathbf{s}^g) is optimized to be close to the discrete prior (\mathbf{y}^g ; Figure 3(b-ii)), as shown in Figure 3(b-iii). This encourages the generative distribution (\mathbf{x}^g) to be close to the separate state, as shown in Figure 3(b-i). In this manner, AC-GAN prefers to learn separate class distributions even when classes overlap.¹

¹Refer to Shu *et al.* [16], who explain these limitations of AC-GAN from a Lagrangian perspective.

3.4 Proposal: CP-GAN

To overcome these limitations, we redesign the generator input and the objective function of AC-GAN, as shown in Figure 2(b). First, to represent the between-class relationship in the generator input, we replace the discrete prior (\mathbf{y}^g) with the classifier’s posterior of real data (\mathbf{s}^r). By this modification, in CP-GAN, the generator is formulated as $\mathbf{x}^g = G(\mathbf{z}^g, \mathbf{s}^r)$.

Second, to render the classifier’s posterior of the generated data (\mathbf{s}^g) close to \mathbf{s}^r instead of discrete \mathbf{y}^g , we reformulate the KL-AC loss of the generated data (Equation 6) as

$$\mathcal{L}_{\text{KL-CP}}^g = \mathbb{E}_{\mathbf{z}^g \sim p^g(\mathbf{z}), \mathbf{x}^r \sim p^r(\mathbf{x})} \mathcal{D}_{\text{KL}}(\mathbf{s}^r \parallel \mathbf{s}^g), \quad (7)$$

where $\mathbf{s}^r = C(\mathbf{y}|\mathbf{x}^r)$ and $\mathbf{s}^g = C(\mathbf{y}|G(\mathbf{z}^g, \mathbf{s}^r))$. We rename the KL-AC loss as the KL-CP loss. By minimizing this loss, G is encouraged to generate data of which classifier’s posterior (\mathbf{s}^g) is close to that of real data (\mathbf{s}^r) in terms of the KL divergence.

An advantage of CP-GAN is that the distribution shape of its generator prior (*i.e.*, \mathbf{s}^r) is determined in a data-driven manner. When real data has class overlaps (Figure 3(a-i)), \mathbf{s}^r represents the class overlapping state (Figure 3(a-iii)). This allows G to generate class-overlapping data (Figure 3(c-i)). When real data is discrete, \mathbf{s}^r also becomes discrete, *i.e.*, close to \mathbf{y}^g . In this case, CP-GAN is close to AC-GAN.

Another advantage is that CP-GAN does not require an additional network, compared with AC-GAN (Figures 2(a) and (b)). Additionally, CP-GAN does not require extra supervision. This means that the calculation cost and the annotation cost are almost the same between AC-GAN and CP-GAN.

Prior GAN (pGAN). As shown in Figure 2(b), when generating an image, CP-GAN requires \mathbf{x}^r to calculate the generator prior $\mathbf{s}^r = C(\mathbf{y}|\mathbf{x}^r)$. To alleviate this requirement, we additionally introduce *prior GAN* (pGAN) that mimics the distribution of \mathbf{s}^r . As shown in Figure 2(c), pGAN has the cGAN formulation [54] and the objective function is defined as

$$\mathcal{L}_{\text{pGAN}} = \mathbb{E}_{(\mathbf{x}^r, \mathbf{y}^r) \sim p^r(\mathbf{x}, \mathbf{y})} [\log D_p(\mathbf{s}^r, \mathbf{y}^r)] + \mathbb{E}_{\mathbf{z}_p^g \sim p_p^g(\mathbf{z}), \mathbf{y}_p^g \sim p_p^g(\mathbf{y})} [\log(1 - D_p(G_p(\mathbf{z}_p^g, \mathbf{y}_p^g), \mathbf{y}_p^g))], \quad (8)$$

where G_p and D_p are a generator and a discriminator, respectively; \mathbf{z}_p^g is the noise sampled from a normal distribution $p_p^g(\mathbf{z}) = \mathcal{N}(0, I)$ and \mathbf{y}_p^g is the class label sampled from a categorical distribution $p_p^g(\mathbf{y}) = \text{Cat}(K = c, p = 1/c)$. When generating an image using pGAN and CP-GAN, we first generate a classifier posterior $\mathbf{s}_p^g = G_p(\mathbf{z}_p^g, \mathbf{y}_p^g)$ using pGAN and subsequently generate an image $\mathbf{x}^g = G(\mathbf{z}^g, \mathbf{s}_p^g)$ using CP-GAN. Note that \mathbf{s}^r is simpler than \mathbf{x}^r ; therefore, it is relatively easy to learn a generator that mimics \mathbf{s}^r . In Section 4, we empirically find that almost no degradation occurs by using $G_p(\mathbf{z}_p^g, \mathbf{y}_p^g)$ instead of \mathbf{s}^r .

3.5 Relationships with previous class-conditional extensions of GANs

In Table 1, we summarize the relationships between CP-GAN and previous class-conditional extensions of GANs, including typical models (*i.e.*, cGAN with a concat discriminator [54] and AC-GAN [58]) and state-of-the-art extensions (*i.e.*, cGAN with a projection discriminator [59] and conditional filtered GAN (CFGAN) [60]). Our technical contributions are three-fold. (1) We incorporate the classifier’s posterior into the generator input to represent the between-class relationships. (2) We redesign the discriminator objective function and introduce the KL-CP loss to make the classifier’s posterior of generated data correspond with that of real data. (3) We additionally introduce pGAN that mimics the classifier’s posterior of real data. As demonstrated in Section 4, these modifications allow the generator to capture the between-class relationships and generate an image conditioned on the class specificity even where the previous class-conditional extensions of GANs fail to do so.

Model	Generator		Discriminator	
	Formulation	Input	Formulation	Objective
AC-GAN [15]	$G(\mathbf{z}^g, \mathbf{y}^g)$	$\mathbf{y}^g \sim \text{Cat}$	$D(\mathbf{x})$ with $C(\mathbf{y} \mathbf{x})$	AC loss
cGAN (concat) [16]	$G(\mathbf{z}^g, \mathbf{y}^g)$	$\mathbf{y}^g \sim \text{Cat}$	$D(\mathbf{x}, \mathbf{y})$	Concat D
cGAN (projection) [15]	$G(\mathbf{z}^g, \mathbf{y}^g)$	$\mathbf{y}^g \sim \text{Cat}$	$D(\mathbf{x}, \mathbf{y})$	Projection D
CFGAN [16]†	$G(\mathbf{z}^g, \mathbf{m}^g)$	$\mathbf{m}^g \sim \text{Mix cond. on } \mathbf{y}^g \sim \text{Cat}$	$D(\mathbf{x}, \mathbf{y})$ with $Q(\mathbf{m} \mathbf{x}, \mathbf{y})$	Cond. MI loss
CP-GAN	$G(\mathbf{z}^g, \mathbf{s})$	$\mathbf{s} = C(\mathbf{y} \mathbf{x}')$ (or $\mathbf{s} = G_p(\mathbf{z}_p^g, \mathbf{y}_p^g)$)	$D(\mathbf{x})$ with $C(\mathbf{y} \mathbf{x})$	KL-CP loss

Table 1: Relationships between CP-GAN and previous class-conditional extensions of GANs. †Naive CFGAN assumes that the number of classes is only two. For comparison purposes, we extend this to class mixture setting.

4 Experiments

In this section, we empirically verify the proposed model on controlled class-overlapping data in Section 4.1 and real class-overlapping data in Section 4.2. Due to the space limitation, we briefly review the experimental setup and only provide the important results in this main text. See the Appendix² and our [website](#) for details and more results.

4.1 Experiments on controlled class-overlapping data

4.1.1 Experimental setup

Dataset. To examine the benchmark performance on our novel task (class-distinct and class-mutual image generation), we used CIFAR-10 [17] in which we constructed the class overlapping states in a controlled manner.³ We consider three settings to cover various situations.

(1) **CIFAR-10** (Figure 4(b)): This is the original CIFAR-10 dataset. We used this setting to confirm whether CP-GAN does not cause a negative effect even in class non-overlapping data. (2) **CIFAR-10to5** (Figure 4(c)): We divided the original **ten** classes ($0, \dots, 9$; defined in Figure 4(a)) into **five** classes (A, \dots, E) with class overlapping. In this setting, class overlapping exists between partial two-class pairs. Hence, classes may overlap (e.g., between A and B) or not overlap (e.g., between A and C). (3) **CIFAR-7to3** (Figure 4(d)): We divided the original **seven** classes ($0, \dots, 6$) into **three** classes (A, B, C) with class overlapping. In this setting, we need to handle three different states: a class-distinct state (e.g., $A \rightarrow 0$), two-class overlap state (e.g., $A \cap B \rightarrow 1$), and three-class overlap state (e.g., $A \cap B \cap C \rightarrow 6$).

Evaluation metrics. We used two evaluation metrics for comprehensive analysis, i.e., class-distinct and class-mutual accuracy (**DMA**) and Fréchet inception distance (**FID**) [18].

(1) **DMA:** To confirm whether a model can generate class-distinct and class-mutual images selectively, we introduced DMA. We first generate an image conditioned on either a class-distinct or class-mutual state, and calculate the accuracy for the expected state. For example, in **CIFAR-10to5** (Figure 4(c)), the class-distinct state for A is represented by \mathbf{y}_A , where \mathbf{y}_X is a one-hot vector denoting the class X . When an image is generated from \mathbf{y}_A , the image is expected to be classified as class 0 (*airplane*). In contrast, the class-mutual state for $A \cap B$ is represented by $(\mathbf{y}_A + \mathbf{y}_B)/2$. When an image is generated from $(\mathbf{y}_A + \mathbf{y}_B)/2$, the image is expected to be classified as class 1 (*automobile*). We compute this accuracy for all class-distinct and class-mutual states and report the average accuracy over all states. (2) **FID:** To assess the generated image quality, we used the FID that measures the distance between p^r and p^g in Inception embeddings.⁴

²In Appendix A, we demonstrate the generality of the proposed model by applying it to image-to-image translation. Appendices B and C provides more results and details of experimental setup, respectively.

³We chose this dataset because it is commonly used both in image generation [16, 17, 18] and in noisy label image classification [8, 64]. For the latter task, class labels are corrupted in a controlled manner, as here.

⁴Another typical metric is the Inception score (IS) [18]. However, its drawbacks have been indicated by the recent studies [18, 19]. Therefore, we used the FID in this study.

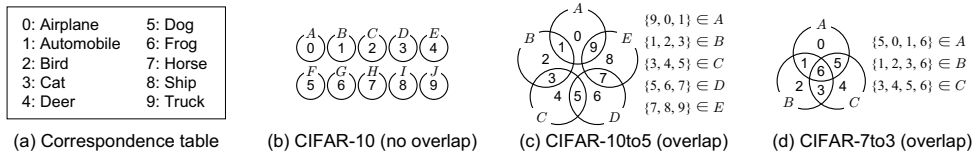


Figure 4: Illustration of class overlapping settings. (a) 0, 1, . . . represent *airplane*, *automobile*, . . . , respectively. (b) This is the original CIFAR-10 dataset (no overlap). In (c) and (d), we divided the original *ten* and *seven* classes into *five* and *three* classes, respectively, following class labels denoted by alphabet letters (A, B, \dots). During the training, we can only use these alphabet class labels and cannot observe the digit class labels (0, 1, . . .).

No.	Condition		CIFAR-10		CIFAR-10to5		CIFAR-7to3	
			DMA \uparrow	FID \downarrow	DMA \uparrow	FID \downarrow	DMA \uparrow	FID \downarrow
1	Dropout	W/	95.4	11.6	77.4	12.2	60.1	13.6
2		W/o	94.8	12.7	51.7	14.9	37.9	18.4
3	# of shared blocks	0	96.8	20.3	56.7	20.9	43.3	23.9
4		1	96.5	19.0	61.0	19.9	40.1	22.4
5		2	94.8	15.3	72.6	15.2	33.9	35.7
6		3	95.7	13.0	78.1	13.6	59.0	16.7
7	Iter. of adding $\mathcal{L}_{\text{KL-CP}}^g$	20k	95.0	12.3	71.2	13.5	49.9	15.4
8		40k	95.8	12.5	63.8	15.0	46.8	14.8
9	λ^g	0.2	96.8	11.2	88.7	12.4	72.2	14.5
10		0.4	97.1	12.0	95.0	12.5	82.0	14.6
11		1	97.4	13.8	96.8	13.9	91.1	15.3

Table 2: Analysis of model configurations. No. 1 is the default model (with dropout, four shared blocks, using $\mathcal{L}_{\text{KL-CP}}^g$ from the beginning, and $\lambda_g = 0.1$). In the other models, only the target parameters are changed. In DMA, the larger the value, the better. In FID, the smaller the value, the better.

4.1.2 Analysis of model configurations

Generalization and memorization. A DNN classifier can memorize even noisy (or random) labels [56]. This is critical for CP-GAN because when C memorizes labels completely, it is difficult to capture between-class relationships. However, appropriately tuned explicit regularization (*e.g.*, dropout) can degrade the training performance on noisy data without compromising generalization on real data [8]. This indicates that it may be possible to learn a well-regularized C in CP-GAN by configuring a model appropriately. To detail this problem, we analyzed model configurations while focusing on the components that affect the regularization of C . We examined three aspects: (1) The effect of **explicit regularization** (*i.e.*, dropout). (2) The effect of a **shared architecture** between D and C . (3) The effect of **joint training** between \mathcal{L}_{GAN} and $\mathcal{L}_{\text{KL-CP}}^g$. We implemented the models based on WGAN-GP ResNet [12] as commonly used benchmarks.

Nos. 1–8 of Table 2 show the results. (1) In the comparison with and without dropout (nos. 1–2), dropout helps to improve both DMA and FID. Regularization by dropout may prevent the models from converging to a few modes (*e.g.*, only class-distinct states) and allow G to capture both class-distinct and class-mutual states. (2) When comparing the number of shared blocks (nos. 1, 3–6), DMA and FID tend to become better (or comparable) as the shared number increases. This indicates that the shared architecture also acts as an effective regularizer. (3) When comparing timing of using $\mathcal{L}_{\text{KL-CP}}^g$ (nos. 1, 7–8), joint training in an early stage (in which C prioritizes learning a simple pattern [8]) helps to improve DMA. Through this analysis, we confirm that explicit regularization, shared architecture, and joint training from the beginning are useful for regularizing C and preventing the memorization.

Effect of trade-off parameter λ^g . Another important parameter that affects the performance is λ^g , which weights the importance between the adversarial loss and the KL-CP

Configuration	GAN	CIFAR-10		CIFAR-10to5		CIFAR-7to3	
		DMA \uparrow	FID \downarrow	DMA \uparrow	FID \downarrow	DMA \uparrow	FID \downarrow
WGAN-GP	AC-GAN	94.9	12.5	36.6	13.7	30.2	14.7
	cGAN	81.0	15.9	32.3	16.9	26.2	18.8
	CFGAN	–	–	50.9	15.8	43.0	16.8
	CP-GAN	97.1	12.0	95.0	12.5	82.0	14.6
SN-GAN	AC-GAN	90.4	12.7	31.4	13.6	30.5	15.5
	cGAN	87.6	10.8	36.2	13.7	27.5	16.6
	CFGAN	–	–	54.5	16.4	43.1	20.8
	CP-GAN	95.2	11.4	64.9	13.0	51.6	15.2

Table 3: Comparing class-conditional extensions of GANs in controlled class-overlapping data.

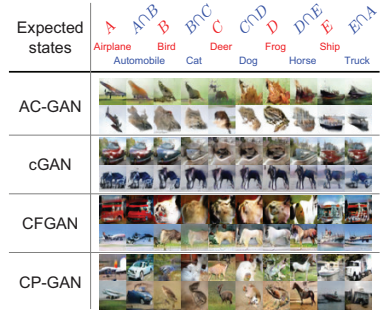


Figure 5: Samples of generated images on CIFAR-10to5. See Figures 8 and 9 in the Appendix for more results.

loss. Nos. 1, 9–11 of Table 2 compare the results for λ^s . We observe a trade-off: the larger λ^s improves the DMA but degrades the FID. However, we find that in class-overlapping cases (*i.e.*, CIFAR-10to5 and CIFAR-7to3), the degradation of the FID is relatively small in $\lambda^s \in [0.1, 0.4]$ while improving the DMA by a large margin.

Effect of pGAN. As discussed in Section 3.4, CP-GAN requires a real \mathbf{x}^r to obtain the generator input \mathbf{s}^r . To mitigate this requirement, we introduced pGAN that instead generates \mathbf{s}^r using randomly sampled variables (*i.e.*, \mathbf{z}_p^s and \mathbf{y}_p^s). Here, we examined the performance of the combination of pGAN and CP-GAN. In particular, we used CP-GAN listed in no. 1 of Table 2. The FID scores for CIFAR-10, CIFAR-10to5, and CIFAR-7to3 are 11.7, 12.2, and 13.7, respectively. They are comparable to the scores in no. 1 of Table 2 (the difference is within 0.1). See Figure 10 in the Appendix, which shows the comparison of \mathbf{s}^r (real classifier’s posterior) and \mathbf{s}_p^s (generated classifier’s posterior using pGAN). This figure also confirms that pGAN can mimic a real classifier’s posterior reasonably well.

4.1.3 Comparison with previous class-conditional extensions of GANs

To verify the effectiveness of CP-GAN, we compared it with three models discussed in Section 3.5: (1) **AC-GAN** [68]; (2) **cGAN** with a projection discriminator [65], which uses $D(\mathbf{x}, \mathbf{y})$ instead of the combination of $D(\mathbf{x})$ and $C(\mathbf{y}|\mathbf{x})$; (3) **CFGAN** [14], with a manually defined class-mixture prior as the generator prior. Unlike CP-GAN, CFGAN requires defining the class-mixture method in advance. We mixed two classes and three classes uniformly for CIFAR-10to5 and CIFAR-7to3, respectively. We did not test CFGAN on CIFAR-10 because this dataset has no class overlaps. We implemented the models based on **WGAN-GP** ResNet [14].⁵ For fair comparison, we also tested **SN-GAN** ResNet [66], which is the optimal GAN configuration for **cGAN**.

Results. We list the results in Table 3. When using WGAN-GP, CP-GAN outperforms the other models in terms of both DMA and FID in all datasets. When using SN-GAN, CP-GAN outperforms the other models in terms of the DMA in all datasets. As of the FID, cGAN achieves the best performance in CIFAR-10. This coincides with the results in [65]. However, we find that it does not necessarily work best in class-overlapping data. Thus, it is important to consider class-distinct and class-mutual image generation separately from typical discrete class-conditional image generation. Figure 5 shows the generated images.

⁵Based on the findings in Table 2, we apply dropout to all models and fix $\lambda^s = 0.4$ in AC-GAN and CP-GAN.

GAN	DA \uparrow	FID \downarrow
AC-GAN	46.3	9.3
cGAN	49.5	11.4
CP-GAN	65.1	6.8

Table 4: Comparing class-conditional extensions of GANs in real-world class-overlapping data.

Expected states	T-Shirt	Shirt	Chiffon	Sweater	Windbreaker	Jacket	Suit	Vest	Underwear					
	Knitwear	Hoodie	Down Coat	Shawl	Dress									
AC-GAN														
	49.5	49.2	23.7	52.4	5.9	27.0	23.8	70.4	81.3	60.5	35.0	60.7	54.3	54.7
cGAN														
	44.8	48.0	25.7	37.6	34.0	35.8	52.5	64.8	73.1	44.9	74.9	52.6	41.8	62.4
CP-GAN														
	51.4	60.2	42.2	55.7	33.6	48.6	86.3	67.9	92.7	67.6	91.9	74.2	70.6	68.1

Figure 6: Samples of generated images on Clothing1M. Number below images indicates the per-class DA. See Figure 11 in the Appendix for more results.

CP-GAN succeeds in selectively generating class-distinct (red font) and class-mutual (blue font) images corresponding with the expected states, whereas the other models fail to do so.

4.2 Experiments on real-world class-overlapping data

We tested CP-GAN on Clothing1M [52], which consists of 14-class clothing images. The data are collected from shopping websites in a real-world scenario and include many mislabels resulting from confusion, as shown in Figure 1(d) (the annotation accuracy is 61.54%). This dataset contains 1M *noisy* and 50k *clean* labeled data as training sets. We used only *noisy* labeled data to address the most realistic setting. Our goal is to construct a generative model that can capture class mixture resulting from confusion and generate class-specific and class-ambiguous images selectively. Based on the findings in Section 4.1, we implemented CP-GAN based on WGAN-GP ResNet [12] and applied dropout (we call this configuration WGAN-GP ResNet-Dropout). We also tested two models as baselines: (1) **AC-GAN** [58] (with WGAN-GP ResNet-Dropout) (2) **cGAN** with a projection discriminator [55] (with SN-GAN ResNet).⁶ To shorten the training time, we resized images from 256×256 to 64×64 . In this dataset, class-mutual states are not given as ground truth; therefore, it is difficult to calculate the DMA. Hence, we instead reported class-distinct accuracy (DA), *i.e.*, we calculated the accuracy only for the class-distinct states (*i.e.*, \mathbf{y}^g is a one-hot vector).

Results. We list the results in Table 4. We confirm that CP-GAN works better than AC-GAN and cGAN in terms of DA and FID even in real-world class-overlapping data. These results indicate that class-overlapping data could cause learning difficulties in previous class-conditional models, and it is important to incorporate a mechanism like ours. We present the qualitative results and per-class DA in Figure 6. CP-GAN succeeds in generating the most class-distinct images in terms of the per-class DA in most cases (12/14). We tested the combination of CP-GAN and pGAN also in this dataset. This achieves the FID of 6.8, which is the same as the score listed in Table 4. See Figure 12 in the Appendix, which shows that pGAN (\mathcal{S}_p^g) can mimic \mathcal{S}^r reasonably well.

⁶We also tested cGAN with WGAN-GP ResNet-Dropout, but we found that it suffers from severe mode collapse during training. Hence, we instead used SN-GAN ResNet, which is an optimal configuration for cGAN.

5 Conclusions

This study introduced a new problem called class-distinct and class-mutual image generation, in which we aim to construct a generative model that can be controlled for class specificity. To solve this problem, we redesigned the generator input and the objective function of AC-GAN, and developed CP-GAN that solves this problem without additional supervision. In the experiments, we demonstrated the effectiveness of CP-GAN using both controlled and real-world class-overlapping data along with a model configuration analysis and a comparative study with state-of-the-art class-conditional extensions of GANs. Based on our findings, adapting our method to other generative models such as VAEs [23, 43], ARs [49], and Flows [9] and using it as a data-mining tool on real-world complex datasets remain interesting future directions.

Acknowledgement. We would like to thank Hiroharu Kato, Atsuhiko Noguchi, and Antonio Tejero-de-Pablos for helpful discussions. This work was supported by JSPS KAKENHI Grant Number JP17H06100, partially supported by JST CREST Grant Number JP-MJCR1403, Japan, and partially supported by the Ministry of Education, Culture, Sports, Science and Technology (MEXT) as “Seminal Issue on Post-K Computer.”

References

- [1] Martin Arjovsky and Léon Bottou. Towards principled methods for training generative adversarial networks. In *ICLR*, 2017.
- [2] Martin Arjovsky, Soumith Chintala, and Léon Bottou. Wasserstein generative adversarial networks. In *ICML*, 2017.
- [3] Devansh Arpit, Stanislaw Jastrzebski, Nicolas Ballas, David Krueger, Emmanuel Bengio, Maxinder S Kanwal, Tegan Maharaj, Asja Fischer, Aaron Courville, Yoshua Bengio, and Simon Lacoste-Julien. A closer look at memorization in deep networks. In *ICML*, 2017.
- [4] Andrew Brock, Jeff Donahue, and Karen Simonyan. Large scale GAN training for high fidelity natural image synthesis. In *ICLR*, 2019.
- [5] Xi Chen, Yan Duan, Rein Houthoofd, John Schulman, Ilya Sutskever, and Pieter Abbeel. InfoGAN: Interpretable representation learning by information maximizing generative adversarial nets. In *NIPS*, 2016.
- [6] Yunjey Choi, Minje Choi, Munyoung Kim, Jung-Woo Ha, Sunghun Kim, and Jaegul Choo. StarGAN: Unified generative adversarial networks for multi-domain image-to-image translation. In *CVPR*, 2018.
- [7] Harm de Vries, Florian Strub, Jérémie Mary, Hugo Larochelle, Olivier Pietquin, and Aaron Courville. Modulating early visual processing by language. In *NIPS*, 2017.
- [8] Emily Denton, Soumith Chintala, Arthur Szlam, and Rob Fergus. Deep generative image models using a Laplacian pyramid of adversarial networks. In *NIPS*, 2015.
- [9] Laurent Dinh, Jascha Sohl-Dickstein, and Samy Bengio. Density estimation using real NVP. In *ICLR*, 2017.

- [10] Vincent Dumoulin, Jonathon Shlens, and Manjunath Kudlur. A learned representation for artistic style. In *ICLR*, 2017.
- [11] Ian J. Goodfellow, Jean Pouget-Abadie, Mehdi Mirza, Bing Xu, David Warde-Farley, Sherjil Ozair, Aaron Courville, and Yoshua Bengio. Generative adversarial nets. In *NIPS*, 2014.
- [12] Ishaan Gulrajani, Faruk Ahmed, Martin Arjovsky, Vincent Dumoulin, and Aaron Courville. Improved training of Wasserstein GANs. In *NIPS*, 2017.
- [13] Kaiming He, Xiangyu Zhang, Shaoqing Ren, and Jian Sun. Deep residual learning for image recognition. In *CVPR*, 2016.
- [14] Zhenliang He, Wangmeng Zuo, Meina Kan, Shiguang Shan, and Xilin Chen. AttGAN: Facial attribute editing by only changing what you want. *arXiv preprint arXiv:1711.10678*, 2017.
- [15] Martin Heusel, Hubert Ramsauer, Thomas Unterthiner, Bernhard Nessler, Günter Klambauer, and Sepp Hochreiter. GANs trained by a two time-scale update rule converge to a Nash equilibrium. In *NIPS*, 2017.
- [16] Sergey Ioffe and Christian Szegedy. Batch normalization: Accelerating deep network training by reducing internal covariate shift. In *ICML*, 2015.
- [17] Takuhiro Kaneko, Kaoru Hiramatsu, and Kunio Kashino. Generative attribute controller with conditional filtered generative adversarial networks. In *CVPR*, 2017.
- [18] Takuhiro Kaneko, Kaoru Hiramatsu, and Kunio Kashino. Generative adversarial image synthesis with decision tree latent controller. In *CVPR*, 2018.
- [19] Takuhiro Kaneko, Yoshitaka Ushiku, and Tatsuya Harada. Label-noise robust generative adversarial networks. In *CVPR*, 2019.
- [20] Tero Karras, Timo Aila, Samuli Laine, and Jaakko Lehtinen. Progressive growing of GANs for improved quality, stability, and variation. In *ICLR*, 2018.
- [21] Tero Karras, Samuli Laine, and Timo Aila. A style-based generator architecture for generative adversarial networks. In *CVPR*, 2019.
- [22] Diederik P Kingma and Jimmy Ba. Adam: A method for stochastic optimization. In *ICLR*, 2015.
- [23] Diederik P Kingma and Max Welling. Auto-encoding variational bayes. In *ICLR*, 2014.
- [24] Diederik P Kingma, Shakir Mohamed, Danilo Jimenez Rezende, and Max Welling. Semi-supervised learning with deep generative models. In *NIPS*, 2014.
- [25] Alex Krizhevsky. Learning multiple layers of features from tiny images. *Technical report*, 2009.
- [26] Ziwei Liu, Ping Luo, Xiaogang Wang, and Xiaoou Tang. Deep learning face attributes in the wild. In *ICCV*, 2015.
- [27] Mario Lucic, Karol Kurach, Marcin Michalski, Sylvain Gelly, and Olivier Bousquet. Are GANs created equal? A large-scale study. In *NeurIPS*, 2018.

- [28] Andrew Maas, Awni Y Hannun, and Andrew Y Ng. Rectifier nonlinearities improve neural network acoustic models. In *ICML Workshop*, 2013.
- [29] Alireza Makhzani, Jonathon Shlens, Navdeep Jaitly, Ian Goodfellow, and Brendan Frey. Adversarial autoencoders. In *NIPS*, 2016.
- [30] Elman Mansimov, Emilio Parisotto, Jimmy Lei Ba, and Ruslan Salakhutdinov. Generating images from captions with attention. In *ICLR*, 2016.
- [31] Xudong Mao, Qing Li, Haoran Xie, Raymond Y.K. Lau, Zhen Wang, and Stephen Paul Smolley. Least squares generative adversarial networks. In *ICCV*, 2017.
- [32] Michael F Mathieu, Junbo Jake Zhao, Junbo Zhao, Aditya Ramesh, Pablo Sprechmann, and Yann LeCun. Disentangling factors of variation in deep representation using adversarial training. In *NIPS*, 2016.
- [33] Lars Mescheder, Andreas Geiger, and Sebastian Nowozin. Which training methods for GANs do actually converge? In *ICML*, 2018.
- [34] Mehdi Mirza and Simon Osindero. Conditional generative adversarial nets. *arXiv preprint arXiv:1411.1784*, 2014.
- [35] Takeru Miyato and Masanori Koyama. cGANs with projection discriminator. In *ICLR*, 2018.
- [36] Takeru Miyato, Toshiki Kataoka, Masanori Koyama, and Yuichi Yoshida. Spectral normalization for generative adversarial networks. In *ICLR*, 2018.
- [37] Vinod Nair and Geoffrey E Hinton. Rectified linear units improve restricted Boltzmann machines. In *ICML*, 2010.
- [38] Augustus Odena, Christopher Olah, and Jonathon Shlens. Conditional image synthesis with auxiliary classifier GANs. In *ICML*, 2017.
- [39] Alec Radford, Luke Metz, and Soumith Chintala. Unsupervised representation learning with deep convolutional generative adversarial networks. In *ICLR*, 2016.
- [40] Scott Reed, Zeynep Akata, Santosh Mohan, Samuel Tenka, Bernt Schiele, and Honglak Lee. Learning what and where to draw. In *NIPS*, 2016.
- [41] Scott Reed, Zeynep Akata, Xinchun Yan, Lajanugen Logeswaran, Bernt Schiele, and Honglak Lee. Generative adversarial text to image synthesis. In *ICML*, 2016.
- [42] Scott Reed, Aäron van den Oord, Nal Kalchbrenner, Victor Bapst, Matt Botvinick, and Nando de Freitas. Generating interpretable images with controllable structure. In *ICLR Workshop*, 2017.
- [43] Danilo Jimenez Rezende, Shakir Mohamed, and Daan Wierstra. Stochastic backpropagation and approximate inference in deep generative models. In *ICML*, 2014.
- [44] Andrés Romero, Pablo Arbeláez, Luc Van Gool, and Radu Timofte. SMIT: Stochastic multi-label image-to-image translation. *arXiv preprint arXiv:1812.03704*, 2018.
- [45] Tim Salimans, Ian Goodfellow, Wojciech Zaremba, Vicki Cheung, Alec Radford, and Xi Chen. Improved techniques for training GANs. In *NIPS*, 2016.

- [46] Rui Shu, Hung Bui, and Stefano Ermon. AC-GAN learns a biased distribution. In *NIPS Workshop*, 2017.
- [47] Luan Tran, Xi Yin, and Xiaoming Liu. Disentangled representation learning GAN for pose-invariant face recognition. In *CVPR*, 2017.
- [48] Dmitry Ulyanov, Andrea Vedaldi, and Victor Lempitsky. Instance normalization: The missing ingredient for fast stylization. In *arXiv preprint arXiv:1607.08022*. 2016.
- [49] Aäron van den Oord, Nal Kalchbrenner, and Koray Kavukcuoglu. Pixel recurrent neural networks. In *ICML*, 2016.
- [50] Aäron van den Oord, Nal Kalchbrenner, Oriol Vinyals, Lasse Espeholt, Alex Graves, and Koray Kavukcuoglu. Conditional image generation with pixelCNN decoders. In *NIPS*, 2016.
- [51] Xiang Wei, Boqing Gong, Zixia Liu, Wei Lu, and Liqiang Wang. Improving the improved training of Wasserstein GANs: A consistency term and its dual effect. In *ICLR*, 2018.
- [52] Tong Xiao, Tian Xia, Yi Yang, Chang Huang, and Xiaogang Wang. Learning from massive noisy labeled data for image classification. In *CVPR*, 2015.
- [53] Bing Xu, Naiyan Wang, Tianqi Chen, and Mu Li. Empirical evaluation of rectified activations in convolutional network. In *ICML Workshop*, 2015.
- [54] Tao Xu, Pengchuan Zhang, Qiuyuan Huang, Han Zhang, Zhe Gan and Xiaolei Huang, and Xiaodong He. AttnGAN: Fine-grained text to image generation with attentional generative adversarial networks. In *CVPR*, 2018.
- [55] Xinchen Yan, Jimei Yang, Kihyuk Sohn, and Honglak Lee. Attribute2image: Conditional image generation from visual attributes. In *ECCV*, 2016.
- [56] Chiyuan Zhang, Samy Bengio, Moritz Hardt, Benjamin Recht, and Oriol Vinyals. Understanding deep learning requires rethinking generalization. In *ICLR*, 2017.
- [57] Han Zhang, Tao Xu, Hongsheng Li, Shaoting Zhang, Xiaogang Wang, Xiaolei Huang, and Dimitris Metaxas. StackGAN++: Realistic image synthesis with stacked generative adversarial networks. *arXiv preprint arXiv:1710.10916*, 2017.
- [58] Han Zhang, Tao Xu, Hongsheng Li, Shaoting Zhang, Xiaogang Wang, Xiaolei Huang, and Dimitris N. Metaxas. StackGAN: Text to photo-realistic image synthesis with stacked generative adversarial networks. In *ICCV*, 2017.
- [59] Han Zhang, Ian Goodfellow, Dimitris Metaxas, and Augustus Odena. Self-attention generative adversarial networks. In *ICML*, 2019.
- [60] Zhifei Zhang, Yang Song, and Hairong Qi. Age progression/regression by conditional adversarial autoencoder. In *CVPR*, 2017.
- [61] Bo Zhao, Bo Chang, Zequn Jie, and Leonid Sigal. Modular generative adversarial networks. In *ECCV*, 2018.
- [62] Junbo Zhao, Michael Mathieu, and Yann LeCun. Energy-based generative adversarial network. In *ICLR*, 2017.
- [63] Jun-Yan Zhu, Taesung Park, Phillip Isola, and Alexei A. Efros. Unpaired image-to-image translation using cycle-consistent adversarial networks. In *ICCV*, 2017.

A Application to image-to-image translation

Our proposed models are general extensions of AC-GAN. Therefore, they can be incorporated into any AC-GAN-based model. To demonstrate this, we incorporate CP-GAN into StarGAN [9], which is a model for multi-domain image-to-image translation. StarGAN is optimized using the AC loss with the adversarial loss [10] and cycle-consistency loss [13]. To combine CP-GAN with StarGAN, we alter the class representation from discrete (\mathbf{y}^g) to classifier’s posterior (\mathbf{s}^r), and replace the AC loss with the KL-CP loss. We call the combined model **CP-StarGAN**. To validate the effectiveness, we employ a modified version of CelebA [26] in which we consider the situation where multiple datasets collected on diverse criteria are given. In particular, we divided CelebA into three subsets: (A) a *black hair* set, (B) *male* set, and (C) *smiling* set. Our goal is to discover class-distinct (e.g., $A \cap \neg B$: *black hair and not male*) and class-mutual (e.g., $A \cap B$: *black hair and male*) representations without relying on any additional supervision. We believe that this would be useful for a real-world application in which we want to discover class intersections for existing diverse datasets.

Results. We present the translated image samples and quantitative evaluation results in Figure 7.⁷ These results imply that CP-StarGAN can selectively generate class-distinct (e.g., $A \cap \neg B \cap \neg C$: *black hair, not male, and not smiling*) and class-mutual (e.g., $A \cap B \cap C$: *black hair, male, and smiling*) images accurately, whereas conventional StarGAN fails. Note that such multi-dimensional attribute representations (e.g., *black hair, not male, and not smiling* ($A \cap \neg B \cap \neg C$)) are not given as supervision during the training. Instead, only the dataset identifiers (i.e., A, B, or C) are given as supervision, and we discover the multi-dimensional representations through learning.

	Input	A	$A \cap B$	B	$B \cap C$	C	$C \cap A$	$A \cap B \cap C$
Expected states	A: Black hair	✓	✓	x	x	x	✓	✓
	B: Male	x	✓	✓	✓	x	x	✓
	C: Smiling	x	x	x	✓	✓	✓	✓

	A	$A \cap B$	B	$B \cap C$	C	$C \cap A$	$A \cap B \cap C$
StarGAN	65.4	54.1	81.6	61.7	88.7	56.9	39.3
CP-StarGAN	76.0	85.3	89.3	92.3	95.4	86.8	91.5

(a) Translated image samples

(b) DMA scores

Figure 7: Samples of translated image and DMA scores on CelebA. We calculate the DMA scores for each class-distinct or class-mutual state. During the training, we only know the dataset identifiers indicated by colorful font, i.e., A (*black hair*), B (*male*), and C (*smiling*). Class-distinct and class-mutual representations (e.g., $A \cap B$; *black hair and male*) are found through learning. See Figure 13 for more samples.

Related work. Recently, class-conditional extensions of GANs were applied to not only to image generation but also to image-to-image translation [6, 14, 44, 51] (including StarGAN [9]). Their goal is to achieve multi-domain image-to-image translation (i.e., to obtain mappings among multiple domains) using few-parameter models. To achieve this, they use the AC-GAN-based loss. Therefore, they suffer from difficulty in applying to class-overlapping data like typical class-conditional image generation models. However, this difficulty can be overcome by replacing the AC-GAN-based loss with CP-GAN-based loss, as shown above.

⁷To calculate DMA, we trained three classifiers (which distinguish male or not, black hair or not, and smiling or not, respectively). We calculated the accuracy for the expected states using these classifiers and reported their average score.

B Extended and additional results

B.1 Extended results of Section 4.1

- Figure 8: Samples of generated images on CIFAR-10, CIFAR-10to5, and CIFAR-7to3. This is the extended version of Figure 5.
- Figure 9: Continuous class-wise interpolation on CIFAR-10to5
- Figure 10: Comparison of the real classifier’s posterior and generated classifier’s posterior using pGAN

B.2 Extended results of Section 4.2

- Figure 11: Samples of generated images on Clothing1M. This is the extended version of Figure 6.
- Figure 12: Comparison of the real classifier’s posterior and generated classifier’s posterior using pGAN

B.3 Extended results of Appendix A

- Figure 13: Samples of translated images on CelebA. This is the extended version of Figure 7.

B.4 Additional results on MNIST

- Figure 14: Samples of generated images on MNIST-3to2, MNIST-10to5, and MNIST-7to3

Expected states	DMA										DMA										DMA												
	A	B	C	D	E	F	G	H	I	J	A	ACB	B	BC	C	CBD	D	DCE	E	EAD	A	ACB	B	BC	C	CBA	ABC						
	Airplane	Bird	Deer	Cat	Dog	Frog	Horse	Ship	Truck	Airplane	Bird	Deer	Frog	Horse	Ship	Truck	Airplane	Bird	Deer	Frog													
AC-GAN											94.9											36.6											30.2
cGAN											81.0											32.3											26.2
CFGAN																						50.9											43.0
CP-GAN											97.1											95.0											82.0
	(a) CIFAR-10 (no overlap)											(b) CIFAR-10to5 (overlap)											(c) CIFAR-7to3 (overlap)										

Figure 8: Samples of generated images on CIFAR-10, CIFAR-10to5, and CIFAR-7to3. This is the extended version of Figure 5. Each row shows samples generated with a fixed z^g and a varied y^g . Each column contains samples generated with the same y^g . CP-GAN succeeds in selectively generating class-distinct (red font) and class-mutual (blue font) images that correspond with the expected states (which are shown in the first row), whereas AC-GAN, cGAN, and CFGAN fail to do so. Note that we do not use class labels of categories (*airplane*, *automobile*, ...) directly as supervision. Instead, we derive them from class labels denoted by alphabet letters (*A, B, ...*). Refer to Figure 4 for the definition of the class overlapping settings.

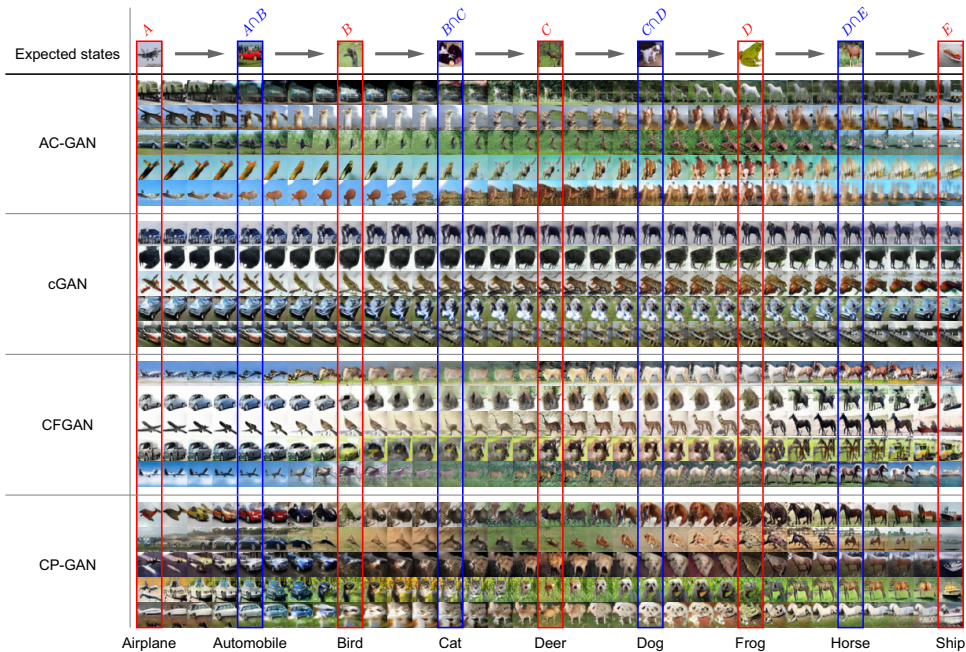
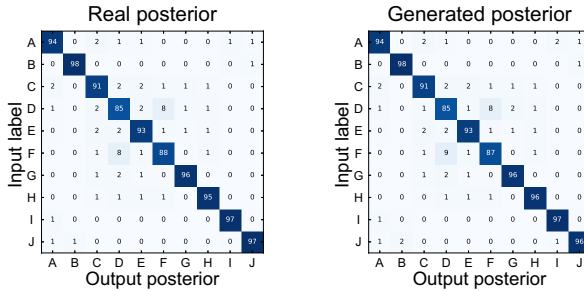
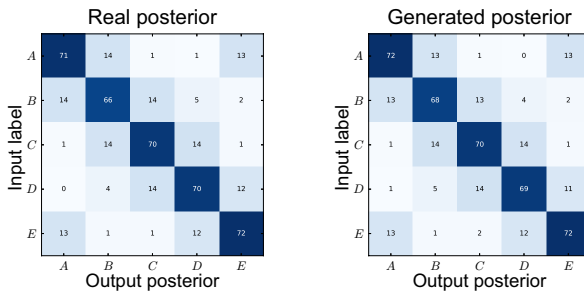


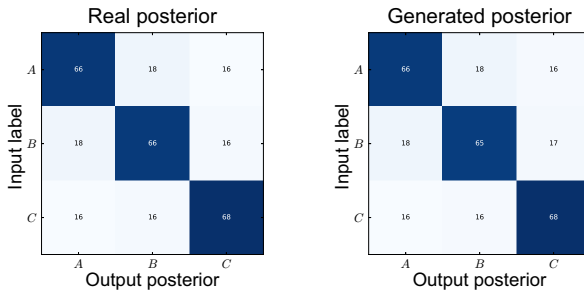
Figure 9: Continuous class-wise interpolation on CIFAR-10to5. In each row, we vary \mathbf{y}^g continuously between classes while fixing \mathbf{z}^g . Even using the previous models (*i.e.*, AC-GAN, cGAN, and CFGAN), it is possible to generate images continuously between classes. However, the changes are not necessarily related to the class specificity. For example, in the fifth column, $A \cap B$ (*automobile*) is expected to appear, but in AC-GAN, unrelated images are generated. In contrast, CP-GAN succeeds in capturing class-distinct (surrounded by red lines) and class-mutual (surrounded by blue lines) images, and can generate them continuously on the basis of the class specificity. For example, from the first to tenth columns, CP-GAN achieves to generate A (*airplane*), $A \cap B$ (*automobile*), and B (*bird*) continuously. As shown in this figure, the aim of class-distinct and class-mutual image generation is different from that of typical class-wise interpolation (or category morphing).



(a) CIFAR-10



(b) CIFAR-10to5



(c) CIFAR-7to3

Figure 10: Comparison of the real classifier’s posterior ($\mathbf{s}^r = C(\mathbf{y}|\mathbf{x}^r)$) and generated classifier’s posterior using pGAN ($\mathbf{s}_p^g = G_p(\mathbf{z}_p^g, \mathbf{y}_p^g)$) in (a) CIFAR-10, (b) CIFAR-10to5, and (c) CIFAR-7to3. The values are averaging over 50k samples. As shown in these figures, pGAN can generate the classifier’s posterior that almost coincides with the real classifier’s posterior, independently of the class-overlapping settings. Additionally, the probability distributions represent the between-class relationships (shown in Figure 4) reasonably well. For example, in CIFAR-10to5, the row *A* has a higher probability in columns *B* and *E* in which the classes overlap. In contrast, it has a lower probability in columns *C* and *D* in which the classes do not overlap.

Expected states	T-Shirt	Shirt	Knitwear	Chiffon	Sweater	Hoodie	Windbreaker	Jacket	Down Coat	Suit	Shawl	Dress	Vest	Underwear	
Real images															DA
AC-GAN															
	49.5	49.2	23.7	52.4	5.9	27.0	23.8	70.4	81.3	60.5	35.0	60.7	54.3	54.7	46.3
cGAN															
	44.8	48.0	25.7	37.6	34.0	35.8	52.5	64.8	73.1	44.9	74.9	52.6	41.8	62.4	49.5
CP-GAN															
	51.4	60.2	42.2	55.7	33.6	48.6	86.3	67.9	92.7	67.6	91.9	74.2	70.6	68.1	65.1

Figure 11: Samples of generated images on Clothing1M for class-distinct states (*i.e.*, \mathbf{y}^g is a one-hot vector). This is the extended version of Figure 6. Each row contains samples generated from a fixed \mathbf{z}^g and a varied \mathbf{y}^g . Each column includes samples generated from the same \mathbf{y}^g . Number below images indicates the per-class DA. The scores confirm that CP-GAN can generate the class-distinct (*i.e.*, more classifiable) images by selectively using the class-distinct states (*i.e.*, \mathbf{y}^g is a one-hot vector).

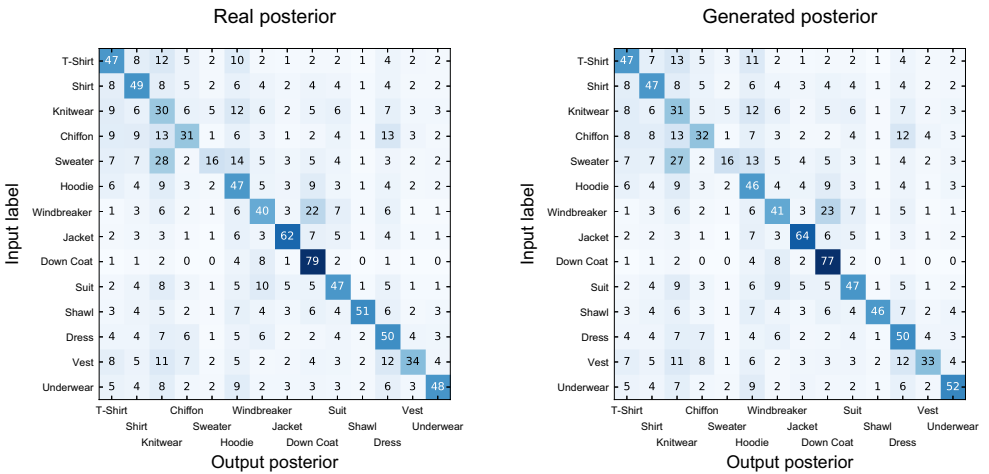


Figure 12: Comparison of the real classifier’s posterior ($\mathbf{s}^r = C(\mathbf{y}|\mathbf{x}^r)$) and generated classifier’s posterior using pGAN ($\mathbf{s}_p^g = G_p(\mathbf{z}_p^g, \mathbf{y}_p^g)$) in Clothing1M. The values are averaging over 50k samples. These figures confirm that pGAN can generate the classifier’s posterior that coincides with the real classifier’s posterior also in the real-world class-overlapping data.

	Input	A	$A \cap B$	B	$B \cap C$	C	$C \cap A$	$A \cap B \cap C$
Expected states	A : Black hair	✓	✓	✗	✗	✗	✓	✓
	B : Male	✗	✓	✓	✓	✗	✗	✓
	C : Smiling	✗	✗	✗	✓	✓	✓	✓
StarGAN								
CP-StarGAN								
StarGAN								
CP-StarGAN								
StarGAN								
CP-StarGAN								
StarGAN								
CP-StarGAN								
StarGAN								
CP-StarGAN								

Figure 13: Samples of translated images on CelebA. This is the extended version of Figure 7. Note that in training, we only know the dataset identifiers indicated by colorful font (i.e., A (black hair), B (male), and C (smiling)) and class-distinct and class-mutual representations (e.g., $A \cap \neg B \cap \neg C$ (black hair, not male, and not smiling)) are found through learning.

Class overlapping setting			
Expected states			
cGAN (Concat)			
cGAN (Projection)			
AC-GAN			
CFGAN			
CP-GAN			
	(a) MNIST-3to2	(b) MNIST-10to5	(c) MNIST-7to3

Figure 14: Samples of generated images on MNIST in class overlapping settings. We consider the situation in which each digit is divided into each class, as shown in the first row. For example, in MNIST-10to5 (b), class A contains digits 0, 1, and 9, and class B contains 1, 2, and 3. During the training, we only used class labels denoted by alphabet letters (A, B, \dots) as supervision. We did not use class labels of digits ($0, 1, \dots$) as supervision. We had to derive them through learning. Each column contains samples generated from the same \mathbf{y}^g . Each row shows generated samples with a fixed \mathbf{z}^g and a varied \mathbf{y}^g . In particular, in (a) we varied \mathbf{y}^g continuously between classes to highlight the difference between typical class-wise interpolation (or category morphing) and class-distinct and class-mutual image generation. Although in the former it is possible to generate images continuously between classes by varying \mathbf{y}^g , the changes are not necessarily related to the class specificity. In contrast, CP-GAN succeeds in selectively generating class-distinct (red font) and class-mutual (blue font) images even when the between-class relationships are not given as supervision.

C Details of experimental setup

In this appendix, we describe the details of the network architectures and training settings for each dataset.

Notation. In the description of network architectures, we use the following notation.

- FC: Fully connected layer
- Conv: Convolutional layer
- Deconv: Deconvolutional (*i.e.*, fractionally strided convolutional) layer
- BN: Batch normalization [16]
- IN: Instance normalization [48]
- ReLU: Rectified unit [57]
- LReLU: Leaky rectified unit [28, 63]
- ResBlock: Residual block [13]

In the description of training settings for GANs, we use the following notation. Note that we used the Adam optimizer [22] for all GAN training.

- α : Learning rate of Adam
- β_1 : The first order momentum parameter of Adam
- β_2 : The second order momentum parameter of Adam
- n_D : The number of updates of D per one update of G

C.1 Toy example

Generative model. The generative model for the toy example (*i.e.*, two-class Gaussian distributions), which was used for the experiments discussed in Section 3.3, is shown in Table 5. As a GAN objective, we used WGAN-GP [12] and trained the model using the Adam optimizer [22] with a minibatch of size 256. We set the parameters to the default values of WGAN-GP for toy datasets,⁸ *i.e.*, $\lambda_{GP} = 0.1$, $n_D = 5$, $\alpha = 0.0001$, $\beta_1 = 0.5$, and $\beta_2 = 0.9$. We set $\lambda^r = 1$ and $\lambda^g = 1$. We trained G for 100k iterations, letting α linearly decay to 0 over 100k iterations.

Generator $G(\mathbf{z}^g, \mathbf{y}^g)$	Discriminator $D(\mathbf{x})$ / Auxiliary classifier $C(\mathbf{y} \mathbf{x})$
$\mathbf{z}^g \in \mathbb{R}^2 \sim \mathcal{N}(0, I) + \mathbf{y}^g$	$\mathbf{x} \in \mathbb{R}^2$
FC \rightarrow 512, ReLU	FC \rightarrow 512, ReLU
FC \rightarrow 512, ReLU	FC \rightarrow 512, ReLU
FC \rightarrow 512, ReLU	FC \rightarrow 512, ReLU
FC \rightarrow 2	FC \rightarrow 1 for D , FC \rightarrow 2 for C

Table 5: Generative model for toy example.

C.2 CIFAR-10

Generative model for CP-GAN. The generative model for CIFAR-10, which was used for the experiments discussed in Section 4.1, is shown in Table 6. We tested two networks:

⁸We refer to the source code provided by the authors of WGAN-GP: https://github.com/igul222/improved_wgan_training.

WGAN-GP ResNet [14]⁹ and SN-GAN ResNet [34].¹⁰ Between these networks, the basic components are the same but the feature size in G (128 in WGAN-GP ResNet but 256 in SN-GAN ResNet) and the global pooling method in D (global mean pooling is used in WGAN-GP ResNet but global sum pooling is used in SN-GAN ResNet) are different. Regarding the dropout position, we also refer to CT-GAN ResNet [51].¹¹ We used conditional batch normalization (CBN) [4, 41] to make G conditioned on y^g . In CP-GAN, to represent class-mixture states, we combined the CBN parameters (*i.e.*, scale and bias parameters) with the weights calculated by the classifier’s posterior. We trained the model using the Adam optimizer [22] with a minibatch of size 64 and 128 for D and G , respectively. We set the parameters to the default values of WGAN-GP ResNet and SN-GAN ResNet, *i.e.*, $n_D = 5$, $\alpha = 0.0001$, $\beta_1 = 0$, and $\beta_2 = 0.9$. We set $\lambda_{GP} = 10$ for WGAN-GP ResNet. We set $\lambda^r = 1$. With regard to λ^g , we compared the performance when alternating the value of the parameter in Table 2. Following [14], in WGAN-GP ResNet, we trained G for 100k iterations, letting α linearly decay to 0 over 100k iterations. Following [34], in SN-GAN ResNet, we trained G for 50k iterations, letting α linearly decay to 0 over 50k iterations.

Generator $G(z^g, y^g)$		Discriminator $D(x)$ / Auxiliary classifier $C(y x)$	
$z^g \in \mathbb{R}^{128} \sim \mathcal{N}(0, I)$, y^g		RGB image $x \in \mathbb{R}^{32 \times 32 \times 3}$	
FC $\rightarrow 4 \times 4 \times ch$		ResBlock down 128	
ResBlock up ch		ResBlock down 128	
ResBlock up ch		0.2 Dropout	
ResBlock up ch		ResBlock down 128	
BN, ReLU		0.5 Dropout	
3×3 stride=1 Conv 3, Tanh		ResBlock 128	
		0.5 Dropout	
		ReLU	
		Global pooling	
		FC $\rightarrow 1$ for D , FC $\rightarrow c$ for C	

Table 6: Generative model for CIFAR-10. In WGAN-GP ResNet, we set $ch = 128$ in G and used global mean pooling in D . In SN-GAN ResNet, we set $ch = 256$ in G and used global sum pooling in D .

Generative model for pGAN. The generative model used for pGAN, is shown in Table 7. We used cGAN with the *concat.* discriminator [34]. The dimension of z_p^g is the same as that of y_p^g . As a GAN objective, we used WGAN-GP [14] and trained the model using the Adam optimizer [22] with a minibatch of size 256. We set the parameters to the default values of WGAN-GP for toy datasets,¹² *i.e.*, $\lambda_{GP} = 0.1$, $n_D = 5$, $\alpha = 0.0001$, $\beta_1 = 0.5$, and $\beta_2 = 0.9$. We trained G_p for 100k iterations, letting α linearly decay to 0 over 100k iterations.

Classifier model used for evaluation. The classifier model used for the CIFAR-10 DMA evaluation is shown in Table 8. We trained the model using the SGD optimizer with a mini-batch of size 128. We set the initial learning rate to 0.1 and divided it by 10 when the iterations are 40k, 60k, and 80k. We trained the model for 100k iterations in total. The accuracy score for the CIFAR-10 test data was 94.7%.

⁹We refer to the source code provided by the authors of WGAN-GP: https://github.com/igul222/improved_wgan_training.

¹⁰We refer to the source code provided by the authors of SN-GAN: https://github.com/pfnet-research/sngan_projection.

¹¹We refer to the source code provided by the authors of CT-GAN: <https://github.com/biuyq/CT-GAN/blob/master/CT-GANs>.

¹²We refer to the source code provided by the authors of WGAN-GP: https://github.com/igul222/improved_wgan_training.

Generator $G_p(\mathbf{z}_p^g, \mathbf{y}_p^g)$	Discriminator $D_p(\mathbf{s}, \mathbf{y})$
$\mathbf{z}_p \in \mathbb{R}^c \sim \mathcal{N}(0, I), \mathbf{y}_p^g$	$\mathbf{s} \in \mathbb{R}^c, \mathbf{y}$
FC \rightarrow 512, ReLU	FC \rightarrow 512, ReLU + \mathbf{y}
FC \rightarrow 512, ReLU	FC \rightarrow 512, ReLU + \mathbf{y}
FC \rightarrow 512, ReLU	FC \rightarrow 512, ReLU + \mathbf{y}
FC $\rightarrow c$	FC \rightarrow 1 for D

Table 7: Generative model for pGAN.

Classifier
RGB image $\mathbf{x} \in \mathbb{R}^{32 \times 32 \times 3}$
3×3 stride=1 Conv 128, BN, ReLU
3×3 stride=1 Conv 128, BN, ReLU
MaxPool
3×3 stride=1 Conv 256, BN, ReLU
3×3 stride=1 Conv 256, BN, ReLU
MaxPool
3×3 stride=1 Conv 512, BN, ReLU
3×3 stride=1 Conv 512, BN, ReLU
3×3 stride=1 Conv 512, BN, ReLU
3×3 stride=1 Conv 256, BN, ReLU
MaxPool
FC \rightarrow 1024, ReLU
0.5 Dropout
FC \rightarrow 1024, ReLU
0.5 Dropout
FC $\rightarrow c$

Table 8: Classifier model used for CIFAR-10 DMA evaluation.

C.3 Clothing1M

Generative model. The generative model for Clothing1M, which was used for the experiments discussed in Section 4.2, is shown in Table 9. As GAN configurations, we used WGAN-GP ResNet [12] for AC-GAN and CP-GAN and used SN-GAN ResNet [36] for cGAN with projection discriminator. We trained the model using the Adam optimizer [22] with a minibatch of size 66. We set the parameters to the default values of WGAN-GP ResNet for 64×64 images,¹³ *i.e.*, $n_D = 5$, $\alpha = 0.0001$, $\beta_1 = 0$, and $\beta_2 = 0.9$. We set $\lambda_{GP} = 10$ for WGAN-GP ResNet. We set the trade-off parameters for the auxiliary classifier to $\lambda^r = 1$ and $\lambda^g = 0.1$. We trained G for 200k iterations.

Classifier model used for evaluation. The classifier model used for the Clothing1M DA evaluation is shown in Table 10. We trained the model using the SGD optimizer with a minibatch of size 129. We set the initial learning rate to 0.1 and divided it by 10 when the iterations are 40k, 60k, and 80k. We trained the model for 100k iterations in total. The accuracy score for clean labeled data was 71.8%.

C.4 CelebA (image-to-image translation)

Generative model. The generative model for CelebA on image-to-image-translation tasks, which was used for the experiments discussed in Appendix A, is shown in Table 11. The

¹³We refer to the source code provided by the authors of WGAN-GP: https://github.com/igul222/improved_wgan_training.

Generator $G(\mathbf{z}^g, \mathbf{y}^g)$		Discriminator $D(\mathbf{x})$ / Auxiliary classifier $C(\mathbf{y} \mathbf{x})$	
$\mathbf{z}^g \in \mathbb{R}^{128} \sim \mathcal{N}(0, I)$, \mathbf{y}^g		RGB image $\mathbf{x} \in \mathbb{R}^{64 \times 64 \times 3}$	
FC $\rightarrow 4 \times 4 \times 512$		3×3 stride=1 Conv 64	
ResBlock up 512		ResBlock down 128	
ResBlock up 256		0.2 Dropout	
ResBlock up 128		ResBlock down 256	
ResBlock up 64		0.2 Dropout	
BN, ReLU		ResBlock down 512	
3×3 stride=1 Conv 3, Tanh		0.5 Dropout	
		ResBlock down 512	
		0.5 Dropout	
		FC $\rightarrow 1$ for D , FC $\rightarrow c$ for C	

Table 9: Generative model for Clothing1M.

Classifier	
RGB image $\mathbf{x} \in \mathbb{R}^{64 \times 64 \times 3}$	
3×3 stride=1 Conv 64, BN, ReLU	
4×4 stride=2 Conv 64, BN, ReLU	
0.5 Dropout	
3×3 stride=1 Conv 128, BN, ReLU	
3×3 stride=1 Conv 128, BN, ReLU	
4×4 stride=2 Conv 128, BN, ReLU	
0.5 Dropout	
3×3 stride=1 Conv 256, BN, ReLU	
3×3 stride=1 Conv 256, BN, ReLU	
4×4 stride=2 Conv 256, BN, ReLU	
0.5 Dropout	
3×3 stride=1 Conv 512, BN, ReLU	
3×3 stride=1 Conv 512, BN, ReLU	
3×3 stride=2 Conv 256, BN, ReLU	
0.5 Dropout	
3×3 stride=1 Conv 512, BN, ReLU	
3×3 stride=1 Conv 512, BN, ReLU	
3×3 stride=1 Conv 256, BN, ReLU	
0.5 Dropout	
FC $\rightarrow c$	

Table 10: Classifier model used for Clothing1M DA evaluation.

network architecture is the same as that of StarGAN [6].¹⁴ As a GAN objective, we used WGAN-GP [22] and trained the model using the Adam optimizer [22] with a minibatch of size 16. We set the parameters to the default values of the StarGAN, *i.e.*, $\lambda_{\text{rec}} = 10$, $\lambda_{\text{GP}} = 10$, $n_D = 5$, $\alpha = 0.0001$, $\beta_1 = 0.5$, and $\beta_2 = 0.999$. We set the trade-off parameters for the auxiliary classifier to $\lambda^r = 1$ and $\lambda^s = 1$. We trained the G for 50k iterations and let α linearly decay to 0 over the last 25k iterations.

Classifier model used for evaluation. The classifier model used for the CelebA DMA evaluation on image-to-image-translation tasks is shown in Table 12. We trained the model using the SGD optimizer with a minibatch of size 128. We set the initial learning rate to 0.1 and divided it by 10 when the iterations are 40k, 60k, and 80k. We trained the model for 100k iterations in total. The accuracy scores for black hair, male, and smiling (binary classification) were 88.4%, 98.5%, and 93.0%, respectively.

¹⁴We refer to the source code provided by the authors of StarGAN: <https://github.com/yunjey/StarGAN>.

Generator $G(x^r, y^g)$	Discriminator $D(x)$ / Auxiliary classifier $C(y x)$
$x^r \in \mathbb{R}^{128 \times 128 \times 3}, y^g$	RGB image $x \in \mathbb{R}^{128 \times 128 \times 3}$
7 × 7 stride=1 Conv 64, IN, ReLU	4 × 4 stride=2 Conv 64, LReLU
4 × 4 stride=2 Conv 128, IN, ReLU	4 × 4 stride=2 Conv 128, LReLU
4 × 4 stride=2 Conv 256, IN, ReLU	4 × 4 stride=2 Conv 256, LReLU
ResBlock 256	4 × 4 stride=2 Conv 512, LReLU
ResBlock 256	4 × 4 stride=2 Conv 1024, LReLU
ResBlock 256	4 × 4 stride=2 Conv 2048, LReLU
ResBlock 256	3 × 3 stride=1 Conv 1 for D
ResBlock 256	2 × 2 stride=1 Conv (zero pad) c for C
4 × 4 stride=2 Deconv 128, IN, ReLU	
4 × 4 stride=2 Deconv 64, IN, ReLU	
7 × 7 stride=1 Conv 3, Tanh	

Table 11: Generative model for CelebA (image-to-image translation).

Classifier
RGB image $x \in \mathbb{R}^{128 \times 128 \times 3}$
3 × 3 stride=1 Conv 32, BN, ReLU
4 × 4 stride=2 Conv 32, BN, ReLU
0.5 Dropout
3 × 3 stride=1 Conv 64, BN, ReLU
4 × 4 stride=2 Conv 64, BN, ReLU
0.5 Dropout
3 × 3 stride=1 Conv 128, BN, ReLU
4 × 4 stride=2 Conv 128, BN, ReLU
0.5 Dropout
3 × 3 stride=1 Conv 256, BN, ReLU
4 × 4 stride=2 Conv 256, BN, ReLU
0.5 Dropout
3 × 3 stride=1 Conv 512, BN, ReLU
3 × 3 stride=1 Conv 512, BN, ReLU
3 × 3 stride=1 Conv 512, BN, ReLU
3 × 3 stride=2 Conv 256, BN, ReLU
0.5 Dropout
FC → c

Table 12: Classifier model used for CelebA DMA evaluation.

C.5 MNIST

Generative model. The generative model for MNIST, which was used for the experiments discussed in Figure 14, is shown in Table 13. As a GAN objective, we used the WGAN-GP [12] and train the model using the Adam optimizer [22] with a minibatch of size 64. We set the parameters to the default values of the WGAN-GP,¹⁵ *i.e.*, $\lambda_{\text{GP}} = 10$, $n_D = 5$, $\alpha = 0.0001$, $\beta_1 = 0.5$, and $\beta_2 = 0.9$. We set the trade-off parameters for the auxiliary classifier to $\lambda^r = 1$ and $\lambda^g = 1$ and trained G for 200k iterations.

Classifier model used for evaluation. The classifier model used for the MNIST DMA evaluation is shown in Table 14. We trained the model using the SGD optimizer with a minibatch of size 128. We set the initial learning rate to 0.1 and divided it by 10 when the iterations are 40k, 60k, and 80k. We trained the model for 100k iterations in total. The accuracy score for the MNIST test data was 99.7%.

¹⁵We refer to the source code provided by the authors of WGAN-GP: https://github.com/igul222/improved_wgan_training.

Generator $G(\mathbf{z}^g, \mathbf{y}^g)$	Discriminator $D(\mathbf{x})$ / Auxiliary classifier $C(\mathbf{y} \mathbf{x})$
$\mathbf{z}^g \in \mathbb{R}^{128}, \mathbf{y}^g$	Gray image $\mathbf{x} \in \mathbb{R}^{28 \times 28 \times 1}$
FC \rightarrow 4096, BN, ReLU	5×5 stride=2 Conv 64, LReLU
Reshape $4 \times 4 \times 256$	0.5 Dropout
5×5 stride=2 Conv 128, BN, ReLU	5×5 stride=2 Conv 128, LReLU
Cut $7 \times 7 \times 128$	0.5 Dropout
5×5 stride=2 Conv 64, BN, ReLU	5×5 stride=2 Conv 256, LReLU
5×5 stride=2 Conv 1, Sigmoid	0.5 Dropout
	FC \rightarrow 1 for D , FC \rightarrow c for C

Table 13: Generative model for MNIST.

Classifier
Gray image $\mathbf{x} \in \mathbb{R}^{28 \times 28 \times 1}$
3×3 stride=1 Conv 64, BN, ReLU
4×4 stride=2 Conv 64, BN, ReLU
0.5 Dropout
3×3 stride=1 Conv 128, BN, ReLU
4×4 stride=2 Conv 128, BN, ReLU
0.5 Dropout
3×3 stride=1 Conv 256, BN, ReLU
3×3 stride=1 Conv 256, BN, ReLU
3×3 stride=1 Conv 256, BN, ReLU
3×3 stride=2 Conv 256, BN, ReLU
0.5 Dropout
FC \rightarrow c

Table 14: Classifier model used for MNIST DMA evaluation.